Influence of Torque on the Lift and Drag of a Particle in an Oscillatory Flow

Paul F. Fischer, [1] Gary K. Leaf, [1] and Juan M. Restrepo*[2]

[1] *Mathematics and Computer Science Division*

Argonne National Laboratory

Argonne, IL 60439, U.S.A.

[2] *Department of Mathematics and Physics Department*

University of Arizona, Tucson, AZ 85721, U.S.A.

April 16, 2008

*Corresponding Author:. restrepo@math.arizona.edu, TEL: (520) 621-4367.

Abstract

In [1] and [2] we computed the lift and drag forces on a sphere, subjected to a wall-bounded oscillatory flow. The forces were found as a function of the Reynolds number, the forcing frequency, and the gap between the particle and the ideally smooth rigid bounding wall. Here we investigate how the forces change as a function of the above parameters and its moment of inertia if the particle is allowed to freely rotate.

Allowing the particle to rotate does not change appreciably the drag force, as compared to the drag experienced by the particle when it is held fixed. Lift differences between the rotating and non-rotating cases are shown to be primarily dominated in the mean by the pressure component. The lift of the rotating particle varies significantly from the fixed-particle case and depends strongly on the Reynolds number, the forcing frequency and the gap; much less so on the moment of inertia. Of special significance is that the lift is enhanced for small Reynolds numbers and suppressed for larger ones, with a clear transition point.

We also examine how the torque changes when the particle is allowed to rotate as compared to when it is held fixed. As a function of the Reynolds number the torque of the fixed sphere is monotonically decreasing in the range $Re = 5$ to $Re = 400$. The rotating-sphere counterpart experiences a smaller and more complex torque, synchronized with the lift transition mentioned before. As a function of the gap, the torque is significantly larger in the fixed particle case.

Keywords: lift, drag, torque, Magnus effect, sphere, wall-bounded flow, oscil-

latory flow.

1 Introduction

The experimental determination of the lift and drag on a particle in a wall-bounded flow is very challenging, as recounted by Rosenthal and Sleath ([3]). In [1] and [2], hereafter referred to as FLR02 and FLR05, respectively, we used instead numerical means to obtain these forces. Our results, which were shown to be consistent with the fluid laboratory experiments of Rosenthal and Sleath, significantly extend the range of parameters for which the lift and drag are now known.

In FLR02 the particle was placed a small distance away from the wall and the forces were then characterized as a function of the forcing frequency and the Reynolds number. The dependence of lift and drag on the forcing frequency, or Keulegan-Carpenter number, was dramatic. The key findings were to show that the lift force is significantly enhanced by the choice of Keulegan-Carpenter number and that the lift, even when compared to a fairly wide range of buoyancy forces, is important in the physical setting. In FLR05 we added the gap number, or distance between the sphere and the bounding wall, to the parameter list. In doing so we found that the sphere experienced suction and repelling effects, depending on the gap number and the forcing frequency. We also found that the nature of the lift force changed from viscous-dominated to pressure-dominated when the Keulegan-Carpenter number, the non-dimensional forcing period, is varied. We also showed that there are only a few degrees of freedom in the spectrum of the forces, suggesting that a reduced but fairly complete analytical model could be formulated for these forces, and such model be accurate for a large range of forcing frequencies.

In the present study we add a rotational degree of freedom to the particle and investigate how lift and drag are modified, as compared to the lift and drag of the same particle, held fixed. We will also quantify the changes in the torque. The primary focus, however, will be to characterize the lift, which we want to describe as a function of the Reynolds number, the forcing frequency, the gap between the sphere and the wall, and the moment of inertia of the particle; the near-term goal is to determine whether rotational freedom will change significantly the amount of lift experienced by a particle, a sensible possibility, at the outset. To suggest that allowing for rotation in the calculation of the lift and drag is of significance is inspired by the work that has been done on flow around circular cylinders. Oscillatory flow around a circular cylinder has been frequently studied: see [4], [5, 6], and references contained in these works. However, as was demonstrated in FLR02 and FLR05, lift and drag estimates from cylinders in an oscillatory flow cannot be extrapolated to the spherical particle case, since the flow is fundamentally different.

The long term goals of this line of inquiry are to provide robust data and functional trends of the basic forces on ideal particles, with which to: (1) infer the mechanics of particle dislodgement and suspension in oscillatory flows, such as those ocurring under the action of of tidal motion, rhythmic sedimentation, and some industrial processes; (2) improve the parametric description of models for what are commonly referred to as "inertial particles" in the sedimentation literature. With regard to the first goal, it would seem that extrapolating sediment dynamic models from what occurs to a single particle is unrealistic. Yet, the basis of some of the most often cited models for the motion of sedimentary/erodible beds in these natural settings rely

on a real or perceived understanding of how individual particles move under the influence of the surrounding fluid, how particles respond to fluid stresses, and how the energy dissipation balance plays out. Of note is that the lift and buoyancy forces enter in the parametrization of dislodgement and/or suspension of the sediment. (See [7] and references contained therein; also see the original work of Bagnold [8], and the extension of this model to the oceanic setting by Bailard in [9]). In any event a thorough study of the single particle in oscillating boundary layer bounded by an ideally smooth bounding wall, we feel, is a necessary first step in tackling the more physically relevant case of a bed of multidispersive particles subjected to oceanic/fluvial hydrodynamics. With regard to the second goal, inertial particle models depend critically on our understanding of how individual as well as finite collections of particles move and interact in a flow (see [10]. Also, [11] for references to the inertial particle literature).

Several studies have considered the forces on a sphere in a free flow. Of note are recent papers on flows over particles forced to rotate. For example, [12] and [13]. See also [14] for an experimental report on the matter. The results from these studies have important practical applications as well as popular interest, for example, the role played by forced spin on the trajectory of baseballs, tennis balls, golf balls. In our study, however, we do not force the particle to spin, but rather, we allow it to freely spin in response to the shearing forces and we ask how the basic forces change by allowing for this degree of freedom.

In [15, 16, 17] the effect of free rotation on the motion of a solid sphere in an unbounded steady shear flow was examined (see also [18]). For flows with moderate Reynolds numbers, from 0.5 to 200, the results most relevant

to our work were their findings that: (1) rotation has little effect on the drag; (2) there is a range of flows wherein the effect of allowing the particle to freely rotate leads to outcomes that are different from existing analytical estimates; (3) the effect of rotation on the lift is Reynolds-number (Re) dependent: for small Re the effect is very small, in accordance with Saffman's results [19, 20]; beyond $Re \approx 200$ the effect again becomes negligible. In the range $Re = 5 - 100$, in particular, they found that the torque-free condition, *i.e.* steady-state, generates a significant increase in the lift. This excess lift is attributed to a Magnus lift effect –of a sphere forced to spin at a rate $\Omega_{st} = \frac{\mathcal{T}}{8\pi\mu D^3}$, the terminal value in a steady shear flow ($\mathcal{T}$ is the torque, D the diameter of the sphere, μ is the viscosity)– and that this excess is additive; (4) at moderate Re they observe that Ω_{st} can be uniquely parameterized by Re alone, yielding a simple power law expression for Ω_{st} as a function of Re.

We show in this study that the results obtained for a sphere that is freely rotating in a wall-bounded oscillatory flow are unlike the results obtained in [15] for the steady shear flow case. Notably, we did not find an obvious way to decompose the forces into a fixed and rotational component, *i.e.* it could not be expressed as the sum of two fields, because the forces change qualitatively with parameters.

Wall-bounded forces on a rigid sphere were examined in [21]. They found that for flows with Reynolds number smaller than 100 the lift decreases with Reynolds number and increases for larger Reynolds number flows. This is unlike the oscillatory flow case we will present. However, the steady flow case they considered and ours have a qualitative similarity with regard to the tendency of the lift to drop as the gap separating the sphere from the wall is increased.

2 Preliminaries

In order to calculate the forces as well as the flow we will be using a high-order spectral element time-dependent Navier-Stokes equations solver. The domain is infinite away from an ideally smooth rigid wall of infinite extent on which the no-slip boundary condition is applied. No-slip boundary conditions for the fluid are applied at the boundary of the sphere as well. The flow is forced to oscillate in time, so that in the absence of the sphere the velocity reverses direction smoothly. The sphere has a fixed diameter of 1 and the fluid has a density of $\rho_0 := 1$ in appropriate dimensional units.

As in FLR02 and FLR05 the Reynolds number is defined as

$$Re := UD/\nu,$$

where the characteristic length-scale D is the particle diameter, and the convective time-scale is D/U. U is the amplitude of oscillation in the far-field velocity and ν is the kinematic viscosity. The nondimensional forcing period, otherwise known as the *Keulegan-Carpenter* number, is

$$\tau := TU/D,$$

where T is the period of the forcing. The *gap* number is

$$\epsilon := d/D,$$

and it represents the ratio of the distance between the edge of the sphere and the wall and D.

In adding a rotational degree of freedom to the particle the flow configuration is now characterized by four parameters: the Keulegan-Carpenter number, the Reynolds number, the gap, and the moment of inertia of the

sphere (which in turn depends on the relative density, for a given diameter D). The dependence of the forces on the relative density

$$R := \rho/\rho_0,$$

will be briefly examined in this study. Here ρ_0 is the density of the fluid.

The computational scheme and parameters are described in FLR02, FLR05. We thus only summarize how the original computational framework is modified to account for the rotating degree of freedom of the sphere. A no-slip boundary condition is enforced at the sphere's surface. The sphere's angular acceleration is derived from

$$\mathbf{T} = I\frac{d\Omega}{dt}, \tag{1}$$

where the torque $\mathbf{T}$ is evaluated by integrating the contributions of the shear stress over the sphere and I is the moment of inertia of the sphere. A second-order Adams-Bashforth scheme

$$\Omega^n = \Omega^{n-1} + \frac{\Delta t}{I}(\frac{3}{2}\mathbf{T}^{n-1} - \frac{1}{2}\mathbf{T}^{n-2}), \tag{2}$$

is used to integrate the angular acceleration. For the density ratios and timestep sizes considered (the latter governed by the standard CFL restrictions arising from explicit treatment of the nonlinear terms in the Navier-Stokes equations no additional stability restrictions on (2) were encountered (see [22]).

The dimensionless torque coefficient, hereon called the normalized torque, is reported in what follows as

$$C_T := \frac{2|\mathbf{T}|}{SD},$$

where

$$S := \frac{1}{2}\rho_0 A U^2,$$

and $A = \pi D^2/4$. In what follows we mean by lift and drag the coefficients $C_L = F_z/S$ and $C_D = F_x/S$, respectively.

In the absence of the sphere the flow field is described analytically as

$$\mathbf{u}_b = \left(\sin(\frac{2\pi t}{\tau}) - e^{-z/\delta}\sin(\frac{2\pi t}{\tau} - z/\delta), 0, 0\right), \tag{3}$$

which corresponds to a unit-amplitude velocity field oscillating back and forth in the x-direction with nondimensional period τ. For viscous flows, this results in a time-periodic boundary layer with characteristic thickness

$$\delta = \sqrt{\frac{\tau}{\pi Re}}.$$

In this study the period is in the range $40 \leq \tau \leq 260$, and thus the Stokes layer range is $0.2 < \delta < 0.96$, for $Re = 100$, which overlaps somewhat with the range of the gap, $0.25 \leq \epsilon \leq 1.0$.

As in FLR02, we use $\mathbf{u} = \mathbf{0}$ as an initial condition in all cases. Mean quantities are reported once the flow has established periodicity in time. The base flow is established by specifying Dirichlet conditions on either end of the domain. When the far-field base flow is in the positive x direction, we set $\mathbf{u}(-L_x, y, z, t) = \mathbf{u}_b$ and use a homogeneous Neumann condition at $x = +L_x$. When the far-field base flow is in the negative x direction, we reverse these conditions. The Neumann condition corresponds to the usual outflow (natural) boundary condition associated with the Stokes subproblem that is solved in each step. Note that the required hydrostatic forcing results directly from application of the boundary conditions and that the auxiliary pressure p_0 is not needed.

3 Torque, Drag, and Lift

Figure 1 depicts the dimensionless velocity profiles (heavy lines) in the boundary layer at different times over the course of the forcing period for $Re = 100$. Figure 1a is representative of the flow for the smaller Keulegan-Carpenter number range; the figure corresponds to $\tau = 80$. Figure 1b, for $\tau = 300$, is representative of the large τ situation. The horizontal lines superimposed on

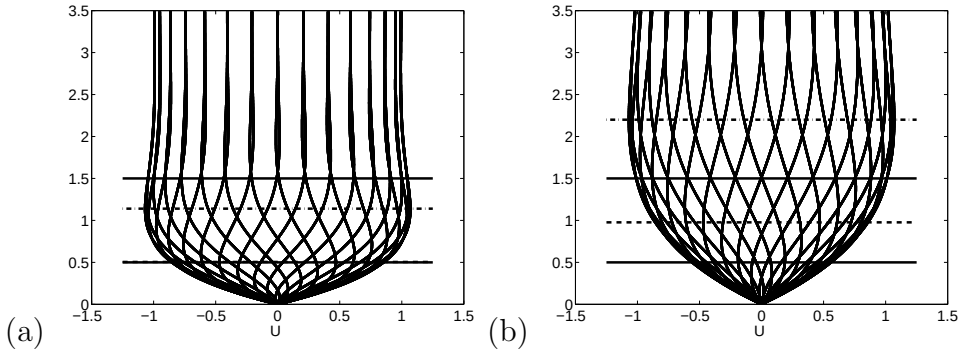

Figure 1: Velocity profiles, given by (3), shown at equal intervals in time over the course of one period of oscillation. $Re = 100$. (a) $\tau = 80$, (b) $\tau = 300$. The horirontal lines depict the top and bottom positions of a unit-diameter-sphere, in (a) for gaps $\epsilon = 0$ (dashed), and $\epsilon = 0.5$ (solid), and in (b) for gaps $\epsilon = 1$ (dashed) and $\epsilon = 0.5$ (solid).

the flow indicate the top and bottom locations of a unit-diameter sphere for several values of the gap ϵ. The vertical scale is D. The size of the boundary layer is, by (3) and in terms of δ, directly proportional to the square root of the velocity amplitude and inversely to the square-root of the period of oscillation. Some aspects of the forces on particles in steady flows (see [15] and references therein) are relevant to shearing flows near boundaries that are more generally time dependent: the time-mean lift force is insignificant

if the particle is placed sufficiently far away from the bounding wall –many δ layer-thicknesses away; that is to say, if the particle is located outside of the boundary layer, there is no shear and thus the lift is insignificant. By the same argument, the larger the boundary layer is relative to the diameter of the sphere provided the particle is close enough to the bounding wall, the higher the shear forces. The presence of the rigid wall also contributes to a Bernoulli effect, which as we shall show, is still evident when the sphere is 1 diameter away from the wall, even if the bulk of the boundary layer is much smaller than the gap. There are fundamental differences between the steady flow and the oscillatory flow situation: the shear rate as inferred from the Figure 1a flow, should lead to a smaller lift than the one inferred from Figure 1b, by steady-flow arguments. Yet, the opposite is true. What is missing from consideration is the addition of a Bernoulli effect in the gap. As we will be showing in the following section, for the range of gaps considered and for large Reynolds numbers, the lift is pressure-dominated.

Bagchi and Balachandar [15] found that the lift of a freely rotating sphere in a steady shear flow will experience an additive lift associated with a Magnus effect. They established this by comparison of their numerical results to a theoretical estimate. When a particle is given a torque-free condition and the flow is oscillating it is not clear how the lift is modified by the added freedom in the motion of the particle. The two aspects that make the outcome hard to predict using prior knowledge about the steady shear case are, (1) if the particle is in a rapidly oscillating shearing flow the particle may not achieve a torque-free condition before the flow reverses; (2) the flow may not be symmetric when there is a reversal in the direction of the force, for example, if vortical structures are generated during the course of the period

and these persist beyond the time at which flow reversal takes place.

In what follows we shall define the *Differential Mean Lift* (DML) as the difference between the mean lift of a particle allowed to rotate and the mean lift of the same particle held fixed. In most instances we will report on relative quantities. For an absolute reference we refer the reader to FLR02 and FLR05.

We describe now how the forces on a particle subjected to an oscillatory boundary layer flow in a torque-free situation depend on the moment of inertia (more specifically on the density ratio R), the Reynolds number Re, the Keulegan-Carpenter number τ and the gap number ϵ.

3.1 Effect of the Density Ratio

We consider here a very small range of density ratios R, because outside of this range we presume that the buoyancy force of a free particle would prevail in the dynamics of a particle in a fluid when compared to the lift force. The dependence of the torque on R was found to be weak. We tried $0.95 \leq R \leq 2$, for $Re = 100$, $\epsilon = 0.5$ and $\tau = 80$. The maximum rotational angle θ_{max} on R is negligible and the peak torque force dependence on R is nearly linear. See Figure 2.

3.2 Sensitivity to the Reynolds Number

The dependence of the lift on the Reynolds number for steady flows was extensively investigated by Bagchi and Balachandar [15, 16]. The definition of Reynolds number in their work is the same as the one adopted in the present study. (See [21] for an investigation of the effect of a nearby wall

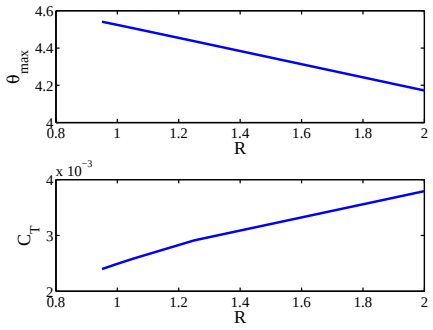

Figure 2: Maximum rotation angle θ_{max} (degrees) and peak normalized torque C_T as a function of R for $Re = 100$, $\epsilon = 0.5$, and $\tau = 80$.

on the lift and drag of a particle). Bagchi and Balachandar found that the lift was sensitive to rotational effects when the Reynolds number was intermediate, in the range $5 \leq Re \leq 100$, approximately, but otherwise it was insensitive to changes in the Reynolds number. They also found that the difference between the fixed and free particles, with respect to the drag, was negligible across the whole range of the Reynolds number. In Figure 3 we show the time series of the drag and lift, angle of deflection (in degrees) and normalized torque, as a function of time, for several values of Re. Figures 3e-f can be contrasted with 3c-d. The lift time series gets considerably more complex as the Reynolds number is increased, developing relatively large high frequency deflections. Comparison of Figures 3c and 3e, as well as Figures 3d and 3f, shows that the complexity in the lift and drag is not as much a function of whether the particle is fixed or torque-free, but primarily a function of Reynolds number. Examination of the fluid flow time series indicates that the complexity in the lift –and to a lesser extent in the drag– has to do with the interactions of the sphere with its own vortical wake. Another feature of the flow is that, as the Reynolds number increases, more

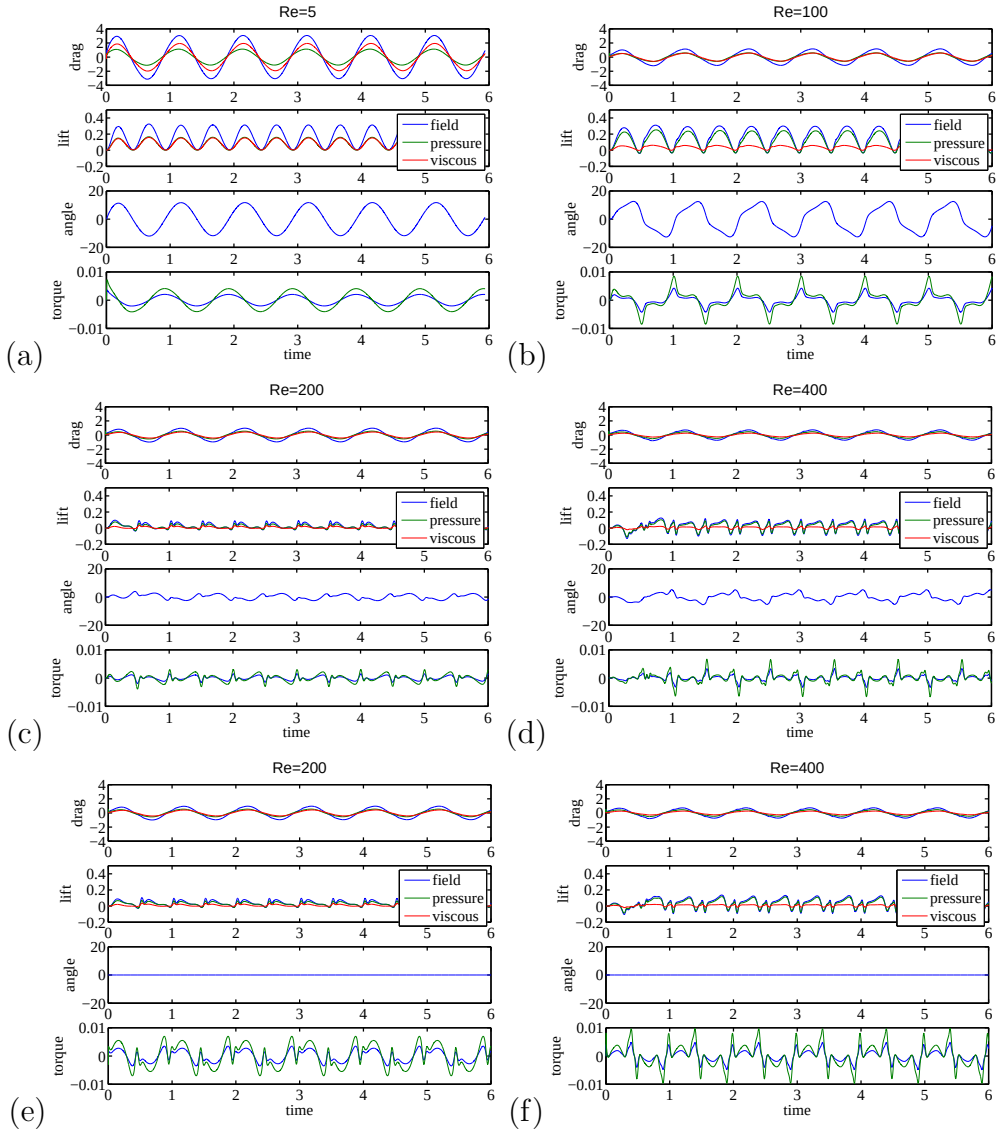

Figure 3: Dependence on Reynolds number. $R = 0.95$, $\tau = 80$, and $\epsilon = 0.25$. Time series of the drag, lift, torque, and angular deflection, for a freely rotating particle: (a) $Re = 5$, (b) $Re = 100$, (c) $Re = 200$, (d) $Re = 400$. For non-rotating particle: (e) $Re = 200$, (f) $Re = 400$.

of the resulting lift and drag is created by the pressure contribution, as compared to the viscous component of the stresses.

It is apparent that the DML in the oscillatory wall-bounded flow case is sensitive in more complex ways to the Reynolds number than in the steady flow case in [15]. Our results appear in Figure 4. The difference between the torque of the non-rotating particle is much larger, for small Re than the rotating counterpart: Figures 4a-b show the torque dependence on the Reynolds number, for the non-rotating and rotating cases, respectively. That it is much

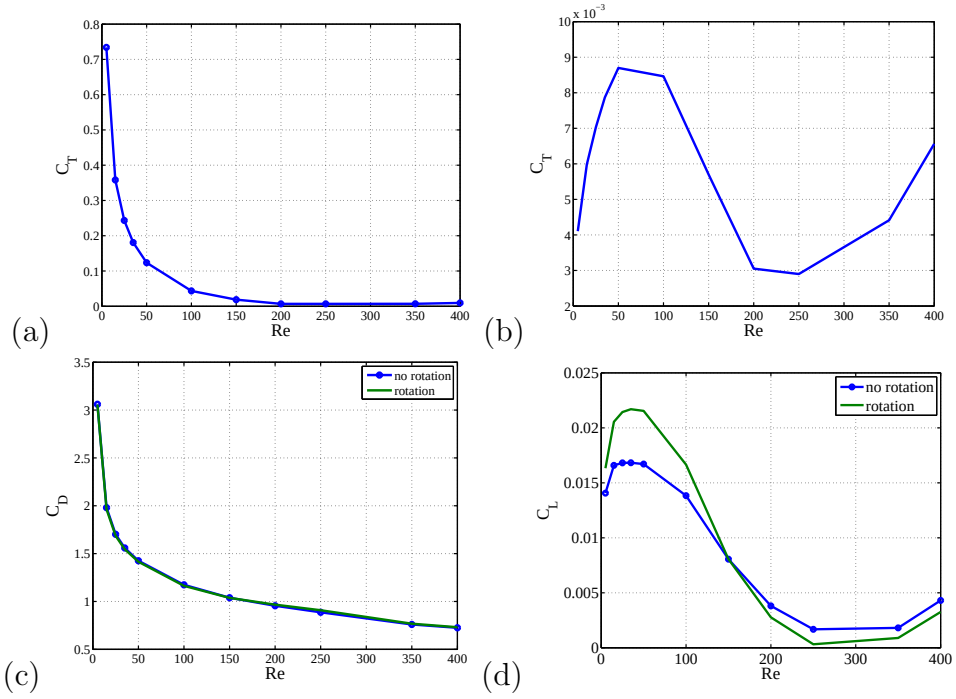

Figure 4: Dependence on the Reynolds number. $R = 0.95$, $\tau = 80$, and $\epsilon = 0.25$. (a) Maximum torque, non-rotating particle, (b) maximum torque of the rotating particle. (c) Maximum drag, with and without rotational effects; (d) the mean lift of the freely rotating and non-rotating cases. The DML is the difference between the two curves in (d).

smaller in magnitude in the rotating case is not surprising, however, that it has a non-monotonic structure is. In Figure 7 we show the dependence of the maximum torque on the gap width and the Keulegan-Carpenter parameter: the torque is small over a large range of Reynolds numbers appears to be true only because the gap was chosen to be large. Figure 4c shows that the drag is nearly equal in the rotating and non-rotating particle cases: symmetry considerations dictate that if the flow is symmetric upon reversals then the maximum and minimum torque values for either the rotating or non-rotating particles should be the same in magnitude, and more importantly, that the difference of the mean drags of both cases should be zero. Figure 4d displays the lift, as a function of the Reynolds number, for the rotating and non-rotating cases: lift is enhanced by rotation for Reynolds numbers below about 150, and a depressed by rotation for Reynolds numbers above 150. Inspection of the vortex field showed that the fields are similar for the rotating and non-rotating cases below $Re = 200$, roughly. In particular, the phase between the features in the vortical field and the forces is more complex; and when a comparison is made between the vorticity of the rotating and non-rotating cases well above $Re = 200$ the fields are different from the lower Reynolds number cases by the appearance of vortical structures. See Figure 5. For $Re \geq 300$ we see that the sphere develops separating vortices on the top of the sphere. Examination of the structure for $Re = 300$ shows two vortex structures separating from the sphere top when the sphere is not rotating. With rotation there are three vortex structures and these are less intense. This also explains why the time series is far more complicated for higher Re, as the passage of the vortices induce fluctuations in the lift and drag.

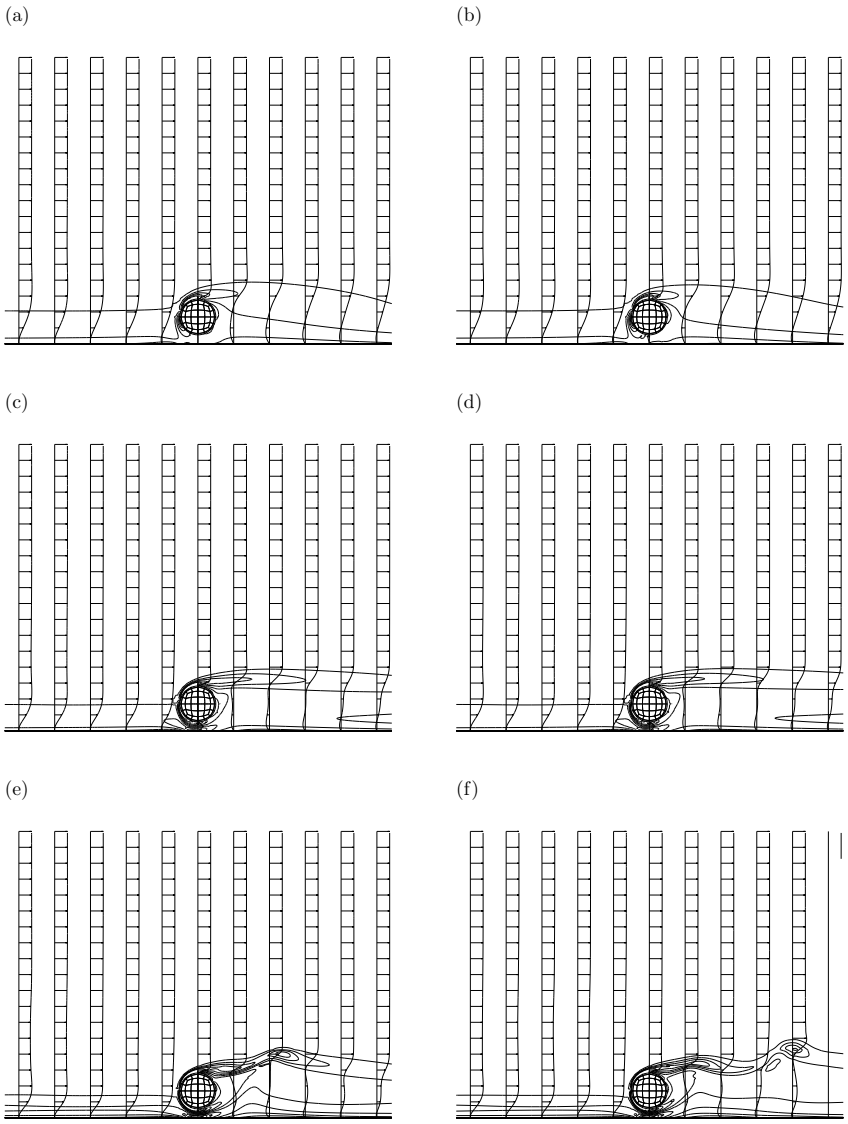

Figure 5: Symmetry-plane velocity profiles and vorticity contours (unit spacing on [-5,5]) during deceleration: (a) $Re = 100$, fixed, (b) $Re = 100$, rotating, (c) $Re = 200$, fixed, (d) $Re = 200$, rotating, (e) $Re = 300$, fixed, (f) $Re = 300$, rotating. $R = 0.95$, $\tau = 80$, and $\epsilon = 0.25$.

The change in the enhancing and depressing effect of rotation on the DML is not as apparent in the vortical plots, but they are in plots of the phase of the lift and drag, as a function of time. Figure 6 shows the lift and drag, as a function of time and of the Reynolds number. These plots

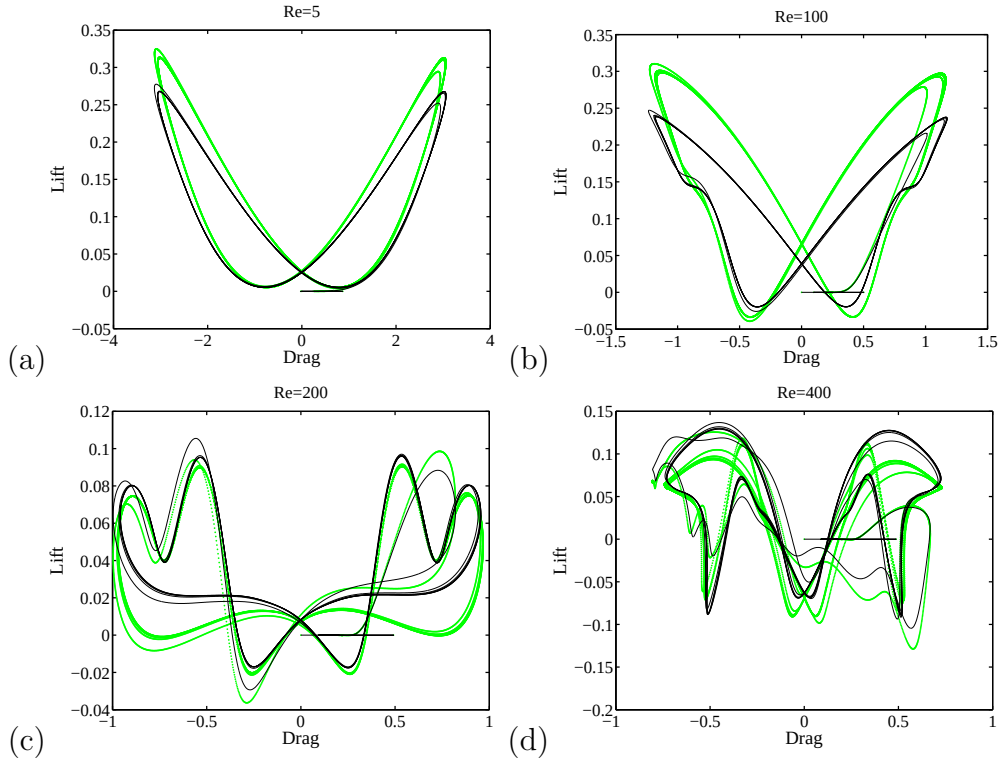

Figure 6: Phase portrait for the instantaneous lift and drag. Dependence on Reynolds number. (a) $Re = 5$, (b) $Re = 100$, (c) $Re = 200$, (d) $Re = 400$. Freely rotating (light), (dark) fixed. $R = 0.95$, $\tau = 80$, and $\epsilon = 0.25$.

do not explain the underlying phenomenon, but do point out that there is a significant portion of the phase tracks (see Figure 6c) in which the lift is considerably smaller in the rotating case than in the fixed case in the range above $Re = 300$.

Parenthetically, in Figure 6d symmetry is significantly affected by the

vortex shedding events.

3.3 Sensitivity to the Keulegan-Carpenter number and the Gap

The angle of deflection θ is more sensitive to changes in the gap ϵ than to the Keulegan-Carpenter number. This is shown in Figure 7a. The high frequency and larger gap cases produce smaller deflection angles. However, as seen from the figure of the maximum normalized torque, Figure 7b, the rate of change of the deflection angle is greater for high frequencies and small gaps, leading to higher torque force values. In Figure 7c we plot the normalized torque for the rotating and non-rotating cases, as a function of τ for a fixed $\epsilon = 0.125$. The difference between the the freely rotating and non-rotating cases for other ϵ is less pronounced.

Figure 8 shows how the DML depends on τ, for various values of ϵ. For small gaps the DML is more important and nearly constant, as a function of τ. Its mean is positive, meaning that the rotation plays a role for small as well as large τ. As the gap is made larger the DML becomes more pronounced as τ increases. For large gaps and small τ the difference between the lift of the rotating and non-rotating cases is less pronounced. In fact, the DML disappears, for a given ϵ and τ. The rightmost disappearance point is approximated by the equation $\tau_c = 320\epsilon - 100$. Below this value rotation adds suction. Above that line the DML is more prominent and gives extra positive lift.

The DML and it pressure and the viscous components appear in Figure 9. The plots indicate that the DML is nearly entirely captured by its pressure

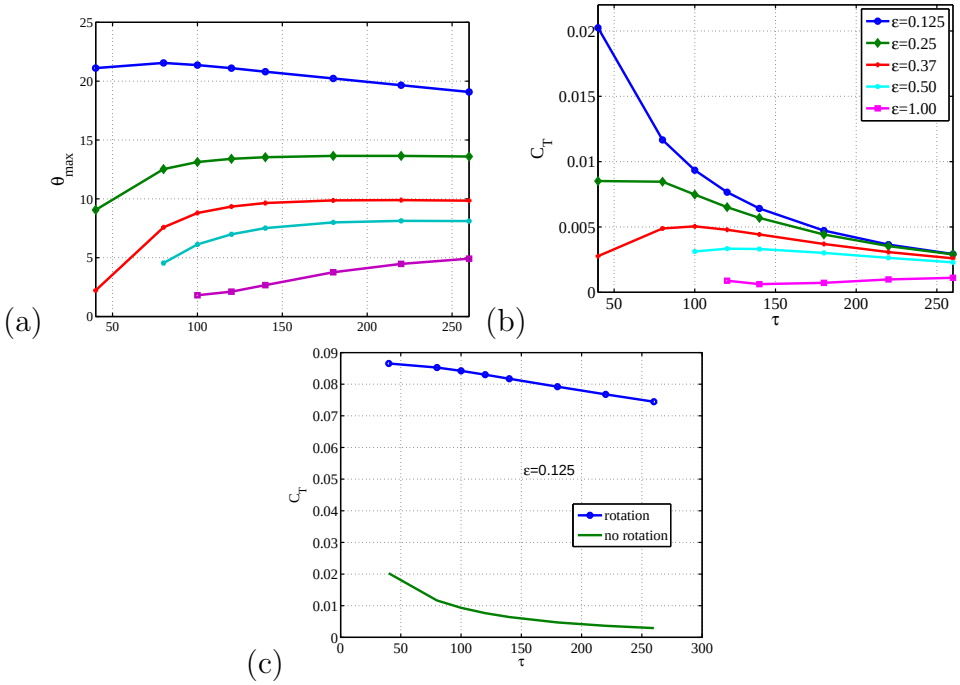

Figure 7: (a) Maximum rotational angle (degrees) and (b) peak normalized torque for the freely rotating sphere, as a function of ϵ and τ. (c) peak normalized torque, comparing the rotating and non-rotating cases for $\epsilon = 0.125$ for all τ. $R = 0.95$, $Re = 100$.

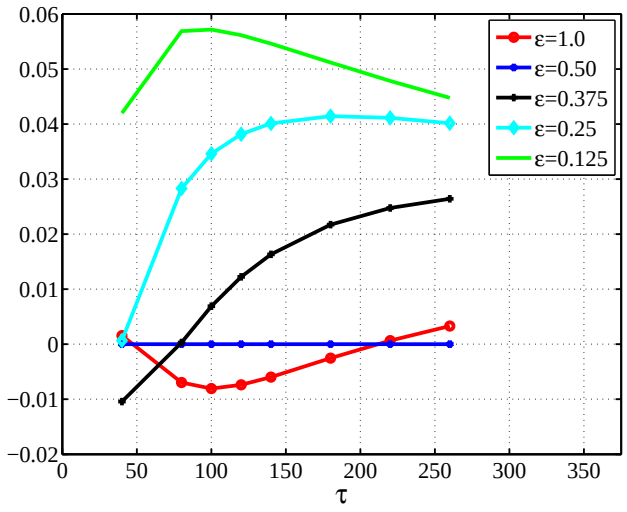

Figure 8: For $Re = 100$, $R = 0.95$, the DML dependence on τ. From top to bottom: $\epsilon = 0.125$, $\epsilon = 0.375$, $\epsilon = 0.5$, $\epsilon = 1.0$.

component, regardless of the gap and period of forcing.

Phase portraits of the forces can be constructed by plotting the drag against the lift forces, for all time. The phase portraits are shown in Figures 10, for $Re = 100$, $R = 0.95$, and low, medium, and large τ. The phase portraits in Figure 10a-c correspond to $\tau = 40$, Figure 10d-f correspond to $\tau = 120$ and Figure 10g-i, to $\tau = 220$. The plots include both the steady state and the transient history and thus are not expected to trace perfectly the same curve over every period. The overall lift decreases sharply with increased gap size and with increased period τ. As the gap gets larger the curves enclose less area and thus the forces are, overall, weaker. But more importantly as the gap gets larger the force maxima go further out of phase, and this effect is not dependent on whether the sphere is allowed to rotate or not. As the τ is increased the two minimas in the lift are seen to flip above $\tau = 120$. For small gap ϵ, the qualitative difference between the rotating

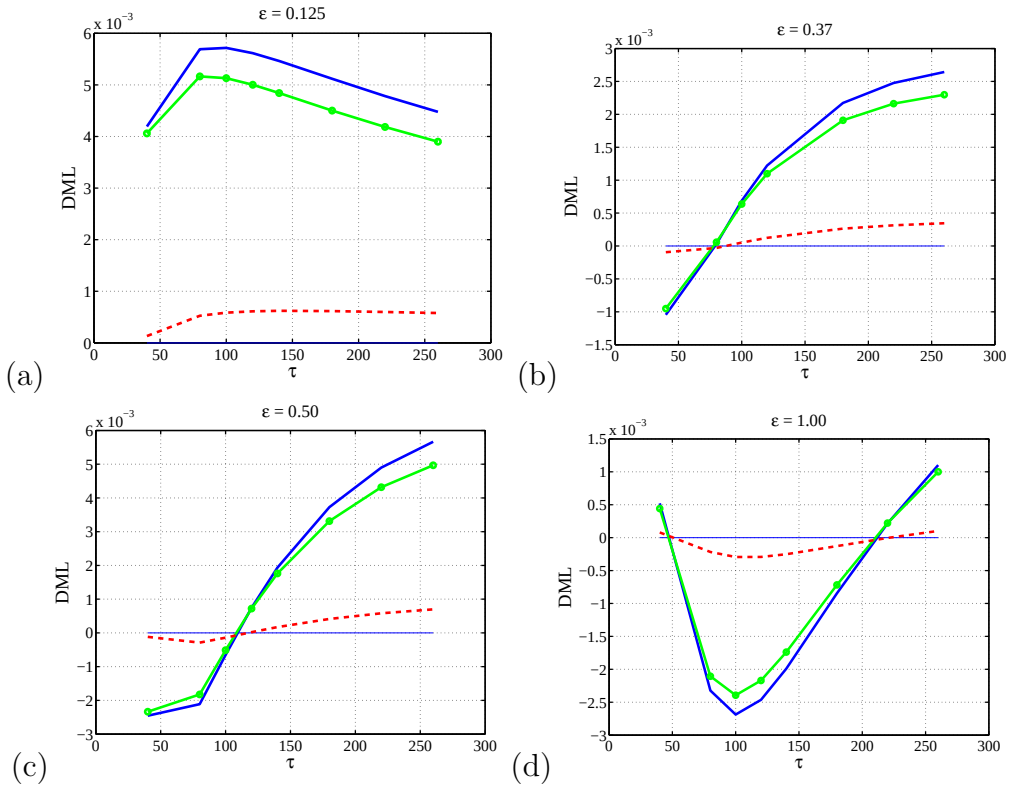

Figure 9: For $Re = 100$, DML (solid), its pressure (circles), and viscous (dashed) components as a function of τ; (a) $\epsilon = 0.125$, (b) $\epsilon = 0.375$, (c) $\epsilon = 0.50$, and (d) $\epsilon = 1.00$.

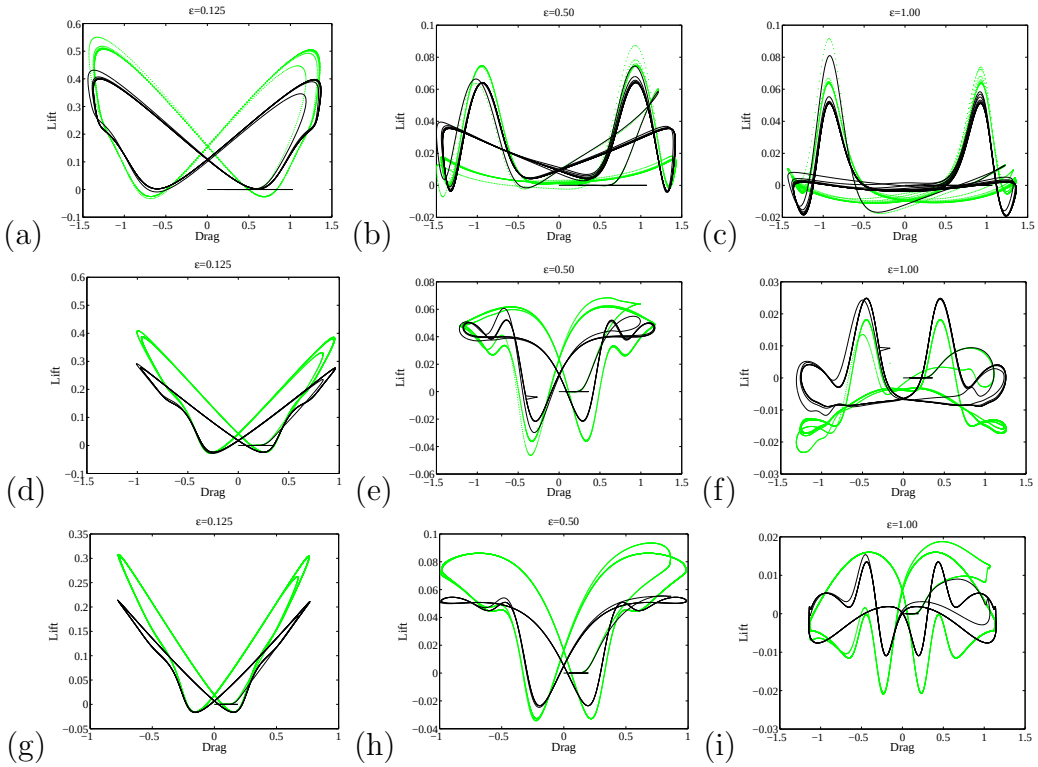

Figure 10: Phase portraits for $\tau = 40$, $Re = 100$, $R = 0.95$, and (a) $\epsilon = 0.125$, (b) $\epsilon = 0.5$, and (c) $\epsilon = 1.00$. Phase portraits for $\tau = 120$, (d) $\epsilon = 0.125$, (e) $\epsilon = 0.5$, and (f) $\epsilon = 1.00$. Phase portraits for $\tau = 220$, (g) $\epsilon = 0.125$, (h) $\epsilon = 0.5$, and (i) $\epsilon = 1.00$. (light) Freely rotating, (dark) fixed.

and non-rotating cases are less pronounced and the variation with τ less pronounced. The small gap the larger differences in the lift occur at the extremes of the drag. In the $\tau = 220$ case we see that the difference between the rotating and non-rotating cases are not topologically different for small ϵ and below the τ_c. Figure 10h is below $\tau = \tau_c$. On the other hand, Figure 10i is radically different and this case is sitting closely to where $\tau = \tau_c$, for this given gap case. For $\tau > \tau_c$ and $\epsilon = 1$ the topology of the phase curve is similar to that of Figure 10h.

Bagchi and Balachandar [15] found negligible differences in the drag experienced by a freely rotating and a non-rotating sphere in a steady shear flow. We find the same type of behavior in the oscillatory shearing case. We thus refer the reader to FLR02 and FLR05 for a summary description on how the drag is affected by the choices in τ and ϵ.

4 Summary

The lift, drag, and torque, on a spherical particle in a oscillatory wall-bounded flow were calculated, as a function of the particle density ratio, the Reynolds number, the Keulegan-Carpenter number and the relative gap between the particle and the wall. The calculations were aimed at elucidating how a rotational degree of freedom affects these forces. In order to do so we calculate the forces on a particle that is held fixed and compare these to the forces obtained when the particle is allowed to freely rotate. These calculations, performed by solving the Navier-Stokes equations in three-dimensions and time, complement the overall picture presented in [1] and [2], on the fundamental forces experienced by a particle in a wall-bounded oscillatory

flow.

With regard to changes in the moment of inertia we found that the difference between the drag and lift of a fixed particle and one allowed to rotate were small. In contrast, the difference between a fixed and freely rotating particle with respect to torque were significant. The torque, not surprisingly, was larger for the fixed particle. The maximum normalized torque is most sensitive to the closeness of the bounding wall when the forcing frequency is large, and is significant for Reynolds numbers smaller than 150, approximately. However, we found that the maximum torque, for low frequencies, is relatively insensitive to the gap size. The maximum normalized torque of a fixed particle was found to be a decreasing function of the Reynolds number. This is not the case for the rotating particle.

The drag force of the freely rotating and the fixed particle are essentially the same, for small Reynolds numbers and variations of all parameters, and insignificantly different for larger Reynolds numbers.

The main focus of this study was the effect of rotation on the lift force. In order to characterize the effect of allowing the particle to freely rotate in response to the flow we focused on the difference between the mean lift of the rotating particle and the mean lift of the particle, fixed in place. This quantity we denoted here as the differential mean lift (DML). We found that the DML is positive for all forcing periods when the gap number is small. As the particle is placed further away from the bounding wall we found that the effective lift is only positive for large Keulegan-Carpenter numbers. We also found that the maximal lift occurs nearly in phase with the maximum drag when the particle is placed close to the wall, but this phase difference increases as the particle is placed further from the wall. Portraits of the drag

and lift forces also indicate that the causal history of the forces is relatively insensitive to the forcing period when the particle is very close to the wall, but becomes sensitive when the particle is placed further away. This last finding, however, is not a result of allowing the particle to rotate: the causal sensitivity is seen both in the rotating and non-rotating particle cases. The overall magnitude of the DML increases as the particle is placed closer to the wall. The DML is pressure-dominated throughout, the Bernoulli effect being significantly different when the particle is fixed as compared to when it is allowed to rotate.

As a function of the Reynolds number we found that for intermediate forcing periods allowing the particle to rotate produced enhanced mean lift, when the Reynolds numbers was small, and depressed mean lift in the large Reynolds numbers regime. We found that this transition occurs approximately at $Re = 150$. When examining the mean lift depression for larger Reynolds numbers we found that the Bernoulli effect alone could not account for the changes in the lift: the sphere induced more vortex shedding from the top of the sphere at high Reynolds numbers, however, the addition of rotation decreases their intensity but increases the number of vortex structures shed. This phenomenology leads to complex histories in the lift. At Reynolds numbers larger than 150 but not not significantly so, the forces of lift and drag are significantly different when the fixed and rotating cases are compared. Specifically, when the lift forces are averaged over the period of the forcing frequency the fact that for large Reynolds numbers the force is insignificant for larger fractions of the period when the particle is rotating is largely responsible for depressed values of the mean lift.

Acknowledgments: This work was carried out in part at Argonne National Laboratory under the auspices of the Department of Energy under Contract DE-AC02-06CH11357. JMR wishes to thank the MCS Division at Argonne, as well as the support by DOE through Grant DE-FG02-03ER25577.

References

[1] P. F. Fischer, G. K. Leaf, and J. M. Restrepo. Forces on particles in an oscillatory boundary layer. *Journal of Fluid Mechanics*, 468:327–347, 2002.

[2] P. F. Fischer, G. K. Leaf, and J. M. Restrepo. Influence of wall proximity on the lift and drag of a particle in an oscillatory flow. *Journal of Fluids Engineering*, 127:583–594, 2005.

[3] G. Rosenthal and J. Sleath. Measurements of lift in oscillatory flow. *Journal of Fluid Mechanics*, 146:449–467, 1986.

[4] P. Justesen. A numerical study of oscillating flow around a circular cylinder. *Journal of Fluid Mechanics*, 222:157–196, 1991.

[5] P. W. Bearman, M. J. Downie, J. M. R. Graham, and E. D. Obajasu. forces on cylinders in viscous oscillatory flow at low Keulegan-Carpenter numbers. *Journal of Fluid Mechanics*, 154:337–356, 1985.

[6] E. D. Obajasu, P. W. Bearman, and J. M. R. Graham. A study of forces, circulation and vortex patterns around a circular cylinder in oscillating flow. *Journal of Fluid Mechanics*, 196:467–494, 1988.

[7] E. M. Lane and J. M. Restrepo. Shore-connected ridges under the action of waves and currents. *Journal of Fluid Mechanics*, 2006.

[8] R. A. Bagnold. Auto-suspension of transported sediment; turbidity. *Proceedings of the Royal Society of London, A*, 265:315–319, 1962.

[9] J. Bailard. An energetics total load sediment transport model for a plane sloping beach. *Journal of Geophysical Research*, 86:10938–10954, 1981.

[10] J. T. Kelly, B. Asgharian, and B. A. Wong. Inertial particle deposition in a monkey nasal mold compared with that in human nasal replicas. *Inhalation Toxicology*, 17:823–830, 2005.

[11] I. J. Benczik, Z. Toroczkai, and T. Teacute. Advection of finite-size particles in open flows. *Physical Review E*, 67:036303, 2003.

[12] D. Kim and H. Choi. Laminar flow past a sphere rotating in the stream-wise direction. *Journal of Fluid Mechanics*, 461:365–386, 2002.

[13] R. Kurose and S. Komori. Drag and lift forces on a rotating sphere. *Journal of Fluid Mechanics*, 384:183–206, 1999.

[14] Y. Tsuji, Y. Morikawa, and O. Mizuno. Experimental measurement of the Magnus force on a rotating sphere at low Reynolds numbers. *Journal of Fluids Engineering*, 107:484–488, 1985.

[15] P. Bagchi and S. Balachandar. Effect of free rotation on the motion of a solid sphere in linear shear flow at moderate Re. *Physics of Fluids*, 14: 2719–2737, 2002.

[16] P. Bagchi and S. Balachandar. Shear versus vortex-induced lift force on a rigid sphere at moderate Re. *Journal of Fluid Mechanics*, 473:379–388, 2002.

[17] P. Bagchi and S. Balachandar. Inertial and viscous forces on a rigid sphere in straining flows at moderate reynolds. *Journal of Fluid Mechanics*, 481:105–148, 2003.

[18] D. R. Mikulencak and J. F. Morris. Stationary shear flow around fixed and free bodies at finite Reynolds number. *Journal of Fluid Mechanics*, 2004.

[19] P. G. Saffman. The lift on a small sphere in a slow shear flow. *Journal of Fluid Mechanics*, 22:385–400, 1965.

[20] P. G. Saffman. (corrigendum) the lift on a small sphere in a slow shear flow. *Journal of Fluid Mechanics*, 31:624, 1968.

[21] L. Zeng, S. Balachandar, and P. Fischer. Wall-induced forces on a rigid sphere at finite Reynolds number. *Journal of Fluid Mechanics*, 536:1–25, 2005.

[22] P. Fischer, F. Loth, S.W. Lee, D. Smith, and H. Bassiouny. Simulation of high Reynolds number vascular flows. *Computer Methods in Applied Mechanics and Engineering*, 196:3049–3060, 2007.

List of Figures